Contents lists available at ScienceDirect

Chemical Engineering Research and Design

journal homepage: www.elsevier.com/locate/cherd

Greener photocatalysts: Hydroxyapatite derived from waste mussel shells for the photocatalytic degradation of a model azo dye wastewater

Jun Haslinda Shariffuddin[a], *Mark Ian Jones*[a], *Darrell Alec Patterson*[b,*]

[a] *Department of Chemical and Materials Engineering, University of Auckland, Private Bag 92019, Auckland Mail Centre, Auckland 1142, New Zealand*

[b] *Laboratory for Nanostructured and Tuneable Materials, Department of Chemical Engineering and Centre for Sustainable Chemical Technologies, University of Bath, Claverton Down, Bath BA2 7AY, United Kingdom*

ABSTRACT

This paper demonstrates for the first time the feasibility of utilising waste mussel shells for the synthesis of hydroxyapatite, $Ca_{10}(PO_4)_6(OH)_2$ (denoted as HAP) to be used as a greener, renewable photocatalyst for recalcitrant wastewater remediation. HAP was synthesised from *Perna canaliculus* (green-lipped mussel) shells using a novel pyrolysis–wet slurry precipitation process. The physicochemical properties of the HAP were characterised using X-ray diffraction (XRD), Fourier transform infrared (FTIR) spectroscopy and scanning electron microscopy (SEM). The HAP produced was of comparable quality to commercial (Sulzer Metco) HAP. The synthesised HAP had good photocatalytic activity, whereby methylene blue (a model textile wastewater compound) and its azo dye breakdown products were degraded with an initial rate of 2.5×10^{-8} mol L^{-1} min^{-1}. The overall azo dye degradation was nearly 54% within 6 h and 62% within 24 h in an oxygen saturated feed in a batch reactor using a HAP concentration of 2.0 g/L, methylene blue concentration of 5 mg L^{-1}, UV irradiation wavelength of 254 nm and a stirring speed of 300 rpm. The kinetics were well described by three first order reactions in series, reflecting the reaction pathway from methylene blue to azo dye intermediates, then to smaller more highly oxidised intermediates and finally degradation of the recalcitrants. The final two steps of the reaction had significantly slower rates than the initial step (rates constants of 6.2×10^{-3} min^{-1}, 1.2×10^{-3} min^{-1} and approximately (due to limited data points) 1.6×10^{-4} min^{-1} for the first, second and third step respectively), which tie in with this mechanism, however it could also indicate that the reaction is either product inhibited and/or affected by catalyst deactivation. FTIR analysis of the post-reaction HAP revealed surface PO_4^{3-} group loss. Since there is good photocatalytic activity with oxygen in limited and excess supply during the photoreaction, this indicates the possibility of lattice oxygen participation in the photocatalytic reaction, which needs to be characterised more fully. However, overall, these results indicate that the HAP derived from the mussel shells is a promising greener, renewable photocatalyst for the photocatalytic degradation of wastewater components.

Keywords: Hydroxyapatite; Photocatalysis; Wastewater treatment; Waste material recycle; Reaction mechanism; Methylene blue

1. Introduction

Mussel farming is a fast growing industry around the world (and especially in New Zealand where this research is based), and the increase in the production of the mussels generates a concomitantly large amount of mussel shell waste. Recent regulations and strategies on the aquaculture waste have opened up new opportunities to sustainable development which has also encouraged the application of environmental technologies (Gaya and Abdullah, 2008; Chong et al., 2010). In particular, mussel shells are a calcium-rich resource that can be used to produce calcium oxide (lime). This lime can

* *Corresponding author*. Tel.: +44 (0)1225386088.
E-mail address: d.patterson@bath.ac.uk (D.A. Patterson).
Received 16 January 2013; Received in revised form 22 March 2013; Accepted 22 April 2013
0263-8762/$ – see front matter © 2013 The Institution of Chemical Engineers. Published by Elsevier B.V. All rights reserved.
http://dx.doi.org/10.1016/j.cherd.2013.04.018

be used in several different ways in environmental technologies, for example in a study conducted by Currie et al. (2007), lime from mussel shells was shown to be able to remove about 90% of phosphates in water. A further study carried out by Abeynaike et al. (2011) indicated that mussel shells can also be converted into hydroxyapatite (HAP) with potential for use as value-added products. Therefore, by utilising shell waste for the purposes of water and wastewater treatment, two existing problems can be solved: pollution remediation and the transformation of a significant existing waste material into a useful commodity.

HAP is widely used in bone regeneration and dental materials since it is the major inorganic component in natural bones and teeth (Sivakumar and Manjubala, 2001; Ji et al., 2009). It has also been widely used as an adsorbent in various applications such as in hydrogenation and wastewater treatment (Zahouily et al., 2003; Reddy et al., 2007). The stoichiometric form of HAP is $Ca_{10}(PO_4)_6(OH)_2$ where the Ca/P molar ratio is 1.67. HAP has been applied as a catalyst in various applications such as for dehydration and dehydrogenation reactions (Abeynaike et al., 2008; Tsuchida et al., 2008; Boucetta et al., 2009; Khachani et al., 2010), synthesis of chalcone derivatives (Solhy et al., 2010), gas-phase oxidation reactions (Jun et al., 2004; Zhang et al., 2008; Domínguez et al., 2009) and also as a photocatalyst in a select few gas-phase photocatalysis processes (Hu et al., 2007; Reddy et al., 2007; Ji et al., 2009; Liu et al., 2010). Very few studies have evaluated HAP as an aqueous phase photocatalyst in its own right – those that have (e.g. Sheng et al., 2011) have only investigated a very limited range of reaction conditions and reactants and have not looked at a wide range of reaction conditions, types of HAP, different reactants and the reaction mechanism. This work therefore aims to begin to fill this knowledge gap, where HAP will be evaluated more extensively than before as an aqueous phase photocatalyst for the remediation of a model dye wastewater containing methylene blue.

Photocatalysis is a rapidly developing wastewater treatment technology, gradually attracting more interest due to its ability to fully mineralise various compounds and so is a potentially important application for HAP. Photocatalysis can be defined as acceleration of a photoreaction by the presence of a catalyst (Mills and Le Hunte, 1997; Gaya and Abdullah, 2008; Castello, 2009). Photocatalysis is best applied when the more common wastewater treatment technologies such as biological degradation, sedimentation, adsorption, flocculation, filtration and reverse osmosis are insufficiently effective (Soon and Hameed, 2011) and where the compound cannot be recovered and needs to be made less toxic and more biodegradable by the photocatalytic oxidative degradation reaction. Three components must be present in order for the heterogeneous photocatalytic reaction to take place: an emitted photon (with appropriate wavelength), a catalytic material (usually a solid catalyst) and a strong oxidising agent which in most cases is oxygen (De Lasa et al., 2005). The most commonly used and most active photocatalysts are powdered semi-conductors such as titanium dioxide (Akpan and Hameed, 2009; Khataee and Kasiri, 2010; Boiarkina et al., 2011) and zinc oxide (Ali et al., 2010, 2011). However the problems with these catalysts are that they are expensive and consist of metals that have limited availability on Earth. Using HAP as a photocatalyst overcomes this problem – it contains readily and widely available atoms (Rakovan, 2002; Al-Qasas and Rohani, 2005), can be made from renewable sources (such as waste mussel shells, as in the present work) and, depending on the required purity, can be inexpensive to make.

In this work the model wastewater compound tested is methylene blue, which is a commonly used compound as the exemplar for azo dye and textile dye wastewaters. It has been extensively studied throughout photocatalysis literature (Houas et al., 2001; Ali et al., 2010, 2011; Boiarkina et al., 2011) and is even the model compound used in the standard method for assessing photocatalysts (Mills, 2012). Therefore it is the ideal compound to benchmark the degradation using the novel HAP photocatalysts synthesised in this work.

Therefore the aim of this paper is to characterise the feasibility of using HAP synthesised from mussel shells as a renewable photocatalyst for the remediation of a model dye wastewater.

2. Materials and methods

2.1. Materials

Green Lipped Mussel shells were kindly donated by Sanford Ltd. (New Zealand) and originate from their Marlborough processing plant. Potassium dihydrogen phosphate (KH_2PO_4) from Sigma–Aldrich (99% pure) was employed in the formation of HAP, methylene blue was obtained from Sigma–Aldrich (85% pure) and 99.5% pure oxygen by BOC gases was used for oxygenation of the reactant solution. A calcium carbonate standard (99.5% purity) was obtained from Sigma–Aldrich. A reagent-grade commercially available HAP powder (Sulzer Metco, Australia) was employed as a comparative standard. All reagents were used as received, unless otherwise stated. The water employed in all the studies was deionised water (from an ELGA Maxima Ultra Purifier System).

2.2. Methods

2.2.1. Synthesis of HAP

Calcium oxide was produced by calcination of waste mussel shells in an in-house fabricated tube furnace under nitrogen flow as described previously (Jones et al., 2011). A wet precipitation method was used in order to prepare the HAP. First, calcium hydroxide with a concentration of 0.1 M was prepared from calcium oxide that was converted from the raw shell, then was left in deionized water overnight in a sealed reactor. A 0.06 M phosphate solution was prepared from potassium dihydrogen phosphate dissolved in deionized water. Specific concentrations for the calcium hydroxide suspension and the phosphate solution were used in order to produce stoichiometric HAP (i.e. HAP with a Ca/P ratio of 1.67). The phosphate solution was added into the HAP reactor by a peristaltic pump (Cole-Parmer MasterFlex, model 7519-06). The solution was stirred over a period of 5 h under a nitrogen atmosphere to produce a milky white suspension containing a precipitate. The resultant solid was separated from the solution by a centrifuge and dried in an oven at 110 °C overnight. The resultant solid is designated as 'as-synthesised HAP'. Part of this material was further processed by heat treatment (pyrolysis in a nitrogen atmosphere in the same tube furnace used for calcination) at 800 °C for 5 h. This material is designated as 'heat treated HAP'.

2.2.2. Photocatalytic degradation experiments

The photocatalysis experiments were carried out in an in-house custom-made stainless steel UV reactor as shown in

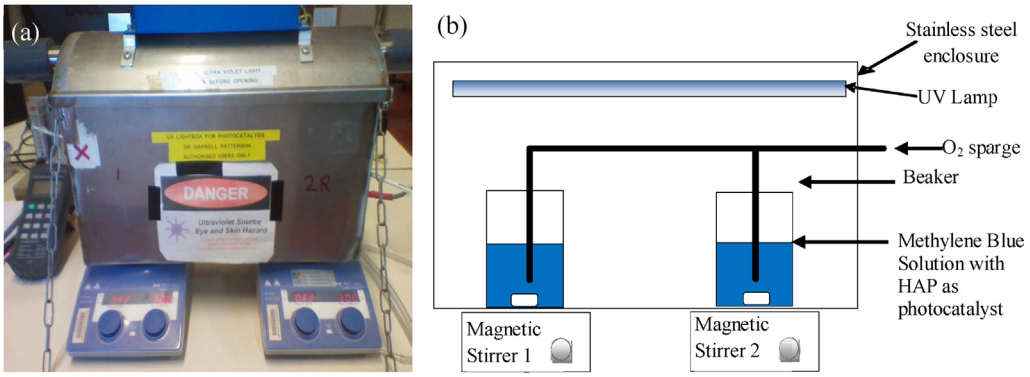

Fig. 1 – (a) Photo of the stainless steel photoreactor enclosure with power supply on top and magnetic stirrers. (b) Schematic of the experimental set-up of the photoreactor, showing the two oxygenated beakers used for the batch photocatalysis experiments.

Fig. 1, described elsewhere (Ali et al., 2010). Two 200 mL beakers were used as reaction vessels. The beakers were filled with 150 mL of methylene blue containing 2.0 g/L of heat treated HAP powder as photocatalyst (as-synthesised HAP was not tested in this work).

Photocatalysis experiments were conducted under both oxygen rich (saturated pure oxygen bubbled into the reaction solution) and oxygen limited (no oxygen bubbled into the reaction solution) conditions. Under limited oxidant supply conditions, the HAP photocatalysts were effectively examined under the 'toughest' reaction regime, where the only oxidant is from the dissolved oxygen within the reaction solution. Additional oxygen can only be provided by mass transfer from the surface of this solution, meaning that the overall reaction rate could be mass transfer limited by the supply of oxidant. In other work (Ali et al., 2010, 2011), this has provided an insight into the oxygen participation during photocatalysis. Prior to illumination, the suspension was magnetically stirred in the dark for 30 min, corresponding to the time needed to establish the adsorption/desorption equilibrium at room temperature. Stirring was maintained to keep the mixture in suspension during the irradiation. At regular intervals, samples of 1.0 mL were withdrawn. Before analysis, the samples were centrifuged to separate the HAP particles. Methylene blue concentration was evaluated by UV–vis spectroscopy (Lambda 35 UV-Visible Perkin Elmer), measuring the peak at 662 nm. Note that this peak does not give a pure response for methylene blue throughout the reaction and will also be contributed to by the absorbance of azo dye photocatalytic reaction intermediates such as Azure A, Azure B and Azure C (Ali et al., 2010, 2011). The strongest response is however from methylene blue, which has its strongest absorbance at this wavelength (see Supplementary material for peak wavelengths comparison of the reaction intermediates), however because of the contributions from the other azo dyes (which are formed by the photocatalytic reaction), the concentration derived from this measurement will be presented and interpreted as 'azo dye' concentration rather than methylene blue alone.

To get a 'pure' concentrations, the aqueous azo dye reaction intermediates and products concentrations (along with a pure methylene blue concentration) were evaluated by high performance liquid chromatography using the method, reagents and instrument detailed in Boiarkina et al. (2011). The concentration of methylene blue was determined by calibration using external standards. Note that UV–vis and HPLC determination of the reaction progress and reaction intermediates and products is used in this work and not measures of mineralisation such as total organic carbon (TOC), since mineralisation is not the aim of this photocatalytic degradation; a partial oxidation to more biodegradable products is. This is desired, since the authors believe that it is a waste of energy and reactor size to fully mineralise wastewater pollutants, when a partial degradation can make most pollutants more biodegradable and therefore amenable to inexpensive and widely available biological wastewater treatment (such as by aerobic and anaerobic digestion in activated sludge wastewater treatment plants). This paper does not address the biodegradability of the products formed however (since this is beyond the scope of the work), but by determining what is being formed (via HPLC) puts the authors in a good position to understand what reaction products are formed when and therefore quantify the extent of partial degradation. Also by knowing the identities of the reaction products, more biodegradable products can be identified through literature search (if required). The biodegradability of the reaction products however is not a focus of the current paper and will be explored in future publications.

The pH of the reaction solution was taken before and after reaction (pH 330i from WTW, Germany). The intensity of the UV lamp was measured using a UV probe (SUV 20.1A2Y2 from IL Metronic Sensortechnik). UV intensity measurements were monitored periodically to ensure a consistent intensity was maintained over the experimental period.

Two sets of control experiments were also conducted under oxygen rich conditions: firstly an evaluation of the photolysis of methylene blue at the same concentrations used during photocatalysis – here reactions were run under equivalent conditions to the photocatalysis runs but in the absence of photocatalyst; secondly reactions were run in the absence of UV (in the dark) over the reaction period to quantify the effect of adsorption over this time.

Note that all reactions were repeated at least once and error bars the mean ± one standard deviation.

2.2.3. *Characterisation of HAP*

Characterisation of the raw shell powder, pyrolysed powder, $Ca(OH)_2$ and HAP produced (both as-synthesised and heat treated), as well as the HAP after the photocatalysis reaction, was carried out using Fourier transform infrared (FTIR) spectroscopy, X-ray diffraction (XRD) analysis and scanning electron microscopy (SEM). FTIR was carried out with a Perkin

Elmer Spectrum 100 using powder on a KRS-5 diamond attenuated total reflectance (ATR) system with the wavenumbers recorded from 380 to 4000 cm^{-1}, in line with other methods used for HAP (Rodriguez-Lorenzo and Vallet-Regi, 2000; Al-Qasas and Rohani, 2005; Mostafa, 2005). The spectra produced were compared to spectra from several references (Koutsopoulos, 2002; Al-Qasas and Rohani, 2005; Resende et al., 2006; Tanaka et al., 2012) allowing the key peaks to be identified.

The X-ray diffraction (XRD) analyses were performed using a Bruker D8 Advance X-ray diffractometer operating with a 40-kV Cu Kα X-ray source. Scans were carried out in the 2θ range of 10°–80° with a 0.02° step size and a 1 s step time.

The morphologies of granular samples were observed using an FEI Quanta 200 FEG scanning electron microscope (5 kV accelerating voltage). Prior to imaging, the samples were double coated with platinum using a Polaron SC 7640 Sputter Coater (2 min coating time) to prevent charging.

3. Results and discussion

3.1. *Conversion of shells to lime by pyrolysis*

Pyrolysis of mussel shells at a temperature of 800 °C results in the decomposition of the limestone as per Eq. (1):

$$CaCO_3 \leftrightarrows CaO + CO_2 \quad (1)$$

The mass loss at 540 °C was consistent with results reported by Jones et al. (2011) where typical mass loss under the calcination temperature of 700 °C was between 3 and 5%. Since there is no lime formed at this temperature, the mass loss can be used to determine the amount of adsorbed moisture and the proteinaceous content of the shell. The pyrolysis of raw shell at 800 °C resulted in mass loss ranging from 44 to 48% including the mass loss of organic material. Subtracting the organic content determined from the mass loss of the sample heated at 540 °C, allows determination of the mass loss during the transformation of carbonate to oxide, and this can be used to determine the extent of transformation from $CaCO_3$ to CaO based on a theoretical mass loss on full conversion of 44%. As shown in Table 1, for these samples the transformation was between 93.6 and 99.5% complete.

Fig. 2 shows XRD patterns for the raw mussel shell powder and powder pyrolysed at 800 °C. For the raw shell powder, all the observed peaks were identified as calcium carbonate with an aragonite crystal structure (Kuriyavar et al., 2000; Nan et al., 2008; Galvan-Ruiz et al., 2009). Following the pyrolysis process at a temperature of 800 °C, the pattern was dominated by peaks from lime, with a small amount of calcium carbonate remaining in the sample in the form of calcite due to the polymorphic transformation of carbonate that takes place when heating the shells above 400 °C (Davis and Adams, 1965; Perić et al., 1996; Resende et al., 2006; Parker et al., 2010; Jones et al., 2011). The FTIR spectra of raw mussel shells and calcium carbonate with 99.5% purity are shown in Fig. 3. Comparing the spectra from a commercial calcium carbonate (with a purity of 99.5%) to the raw shells, the sharp intense bands around 1400 cm^{-1}, 877 cm^{-1} and 700 cm^{-1} confirm a very close similarity. These bands correspond to the C—O bond from carbonate (Kuriyavar et al., 2000; Nan et al., 2008; Galvan-Ruiz et al., 2009). In addition, the bands around 700–704 cm^{-1} correspond to an aragonite polymorph (Kuriyavar et al., 2000; Nan et al., 2008). The FTIR spectrum in 3(c) shows a band around

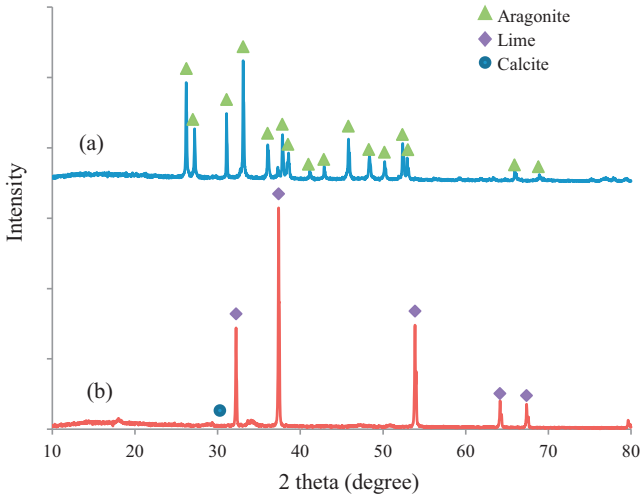

Fig. 2 – XRD patterns demonstrating the change in crystal structure and chemical composition of pyrolysed mussel shell powder: (a) 75–150 μm raw mussel shell (b) 75–150 μm mussel shell pyrolysed at 800 °C.

3640 cm^{-1} attributed to hydroxyl stretching where this band appears due to adsorbed water and —OH species perturbed due to hydrogen bonding (Resende et al., 2006; Galvan-Ruiz et al., 2009). The band at 1416 corresponds to C—O bond from carbonate while the band around 875 cm^{-1} and 500 cm^{-1} corresponds to Ca—O bonds (Galvan-Ruiz et al., 2009). This again indicates that lime has formed with an unconverted calcium carbonate residual.

The SEM images shown in Fig. 4 indicate that there are structural changes that occur during the pyrolysis, consistent with those observed in previous studies (Abeynaike et al., 2011; Jones et al., 2011). Fig. 4a and c show that the raw mussel shells have well-defined edges and are fragmented to reveal a layered structure common in mollusks. In Fig. 4b, it can be seen that the edges were not well-defined. In Fig. 4d, it can be seen that there are some relief lines on the particle surfaces resulting from the high temperature during calcination.

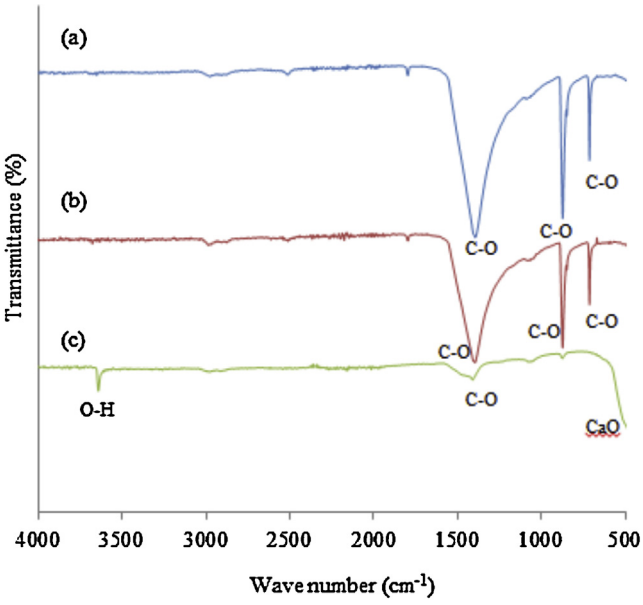

Fig. 3 – FTIR spectra of (a) calcium carbonate with 99.5% purity, (b) raw mussel shells and (c) mussel shells pyrolysed at 800 °C.

Table 1 – Summary of mass loss from raw shell and calcium carbonate with 99.5% purity.

Item	Pyrolysis temp. (°C)	Holding time (h)	Mass loss[a] (%)	Transformation[b] (%)
Raw shell	540	3	4.6	0
Raw shell	800	5	44–48	93.6–99.5
$CaCO_3$ with 99.5% purity	800	5	41.6	94.5

[a] Total percentage of mass loss includes the organic material.
[b] Total percentage of transformation takes into consideration the mass loss due to organics.

For the pyrolysed shells, the coarsening of particles can be observed as shown in Fig. 4b and d. The morphology of the raw mussel shells differed considerably from the calcium oxide indicating that the calcination process releases CO_2 as shown in Eq. (1) and creates some cavities. This structure of the calcined shells helps to react with deionised water to hydrolyse the calcium oxide to calcium hydroxide in order to form a solid suspension/slurry of calcium hydroxide for the preparation of HAP.

3.2. *Formation of HAP from the shell-derived lime*

HAP was synthesised in a semi-batch reactor via a heterogeneous reaction where the potassium dihydrogen phosphate was being dosed into a stirred solid suspension of calcium hydroxide. The precipitates from the reaction were washed several times using deionised water and further dried overnight in an oven at 110 °C. The overall reaction for this mechanism is shown by Eq. (2):

$$10Ca(OH)_2 + 6KH_2PO_4 \leftrightarrows Ca_{10}(PO_4)_6(OH)_2 + 6KOH + 12H_2O \quad (2)$$

Characterisation of as-synthesised and heat treated powders by FTIR and XRD (Figs. 5 and 6) confirmed that HAP was produced. The XRD pattern for the as-synthesised HAP (Fig. 5a) confirms that although HAP was formed (full peak match to reference XRD patterns as reported by Koutsopoulos, 2002; Al-Qasas and Rohani, 2005; Tsuchida et al., 2008; Wang et al., 2010), there was still a small trace of calcite remaining from the original calcination process since the transformation of the raw shell to lime is between 93.6 and 99.5% as shown in Table 1. Similar findings were observed in the FTIR spectrum

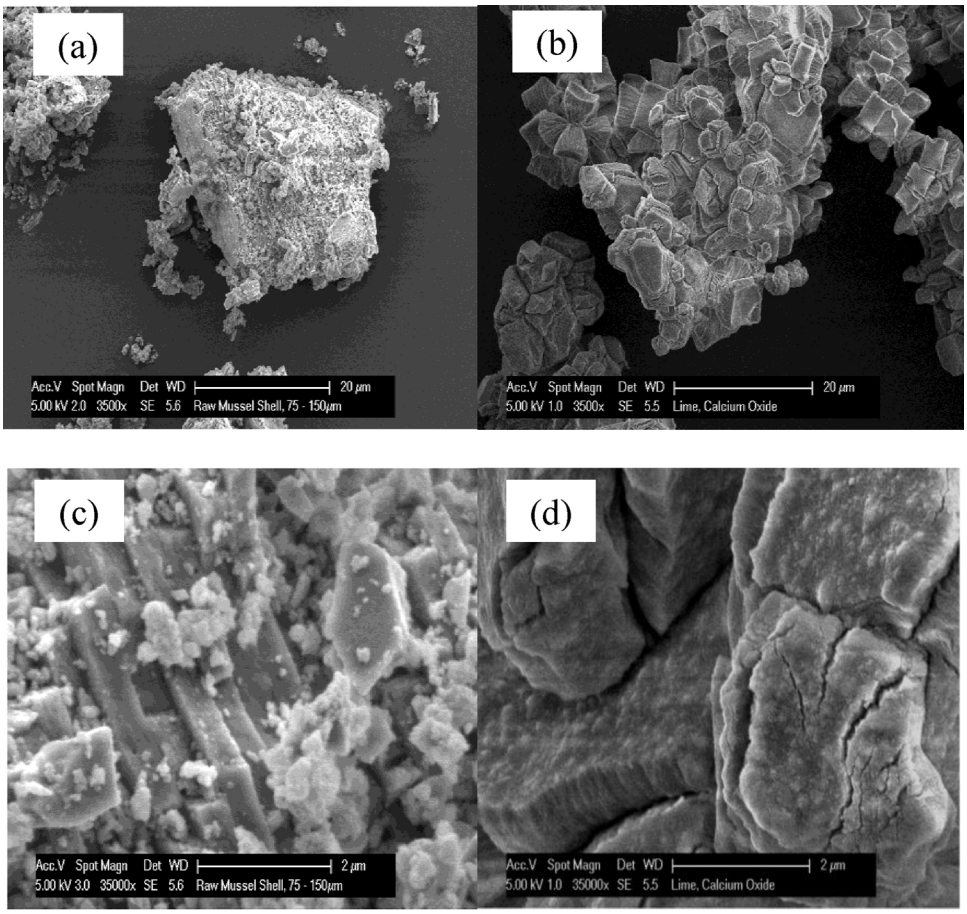

Fig. 4 – SEM micrographs of (a) overall view of a raw mussel shell particle after crushing and grinding, (b) overall view of a calcium oxide particle produced from shell pyrolysed at 800 °C, (c) close-up of the surface morphologies of the raw mussel shell, (d) close-up of the surface morphologies of the pyrolysed at 800 °C.

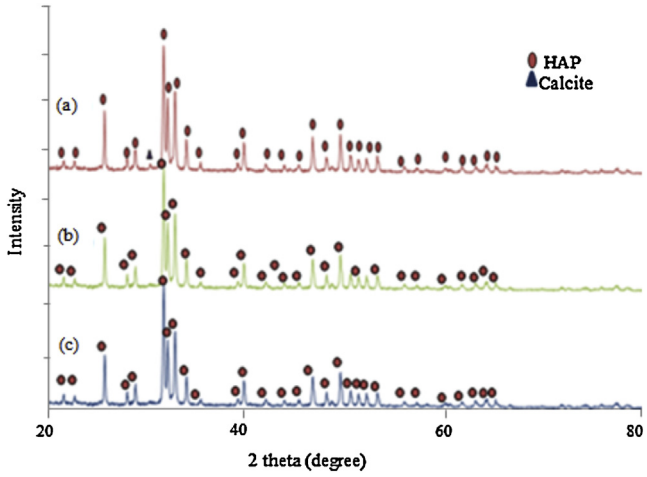

Fig. 5 – XRD patterns for three different HAP powders: (a) as-synthesised HAP, (b) heat treated HAP, and (c) Commercial HAP.

for the as-synthesised HAP as shown in Fig. 6a where the band at 1417 cm^{-1} corresponds to the CO_3^{2-} group. The existence of CO_3^{2-} ions in the HAP could also be due to the adsorption of CO_2 in the atmosphere during the preparation of HAP (Rodriguez-Lorenzo and Vallet-Regi, 2000; Tanaka et al., 2012; Khalid et al., 2013). It should be noted that the synthesis of HAP done in this work were done in a nitrogen atmosphere in order to minimise the possibilities of the incorporation of the CO_3^{2-} in the lattice (via CO^2 uptake). The calcite was not detected for the heat treated HAP as shown by the XRD pattern in Fig. 5b however, either indicating that some of the remain calcite was converted to lime via calcination during this final heat treatment as in previous work (Jones et al., 2011), or that the calcite or lime (that is expected to form in the heat treated HAP) could not be detected by the XRD – the XRD detection limit is 5–10% (Cullity, 1956). Note that Khalid et al. (2013) has similar findings on the decrease in the intensity of CO_3^{2-} ions in the FTIR spectrum when HAP powders were heat treated.

The FTIR analyses for the as-synthesised, heat treated and commercial (Sulzer Metco) HAP shown in Fig. 6 again confirmed that HAP was formed from the shell material, with the

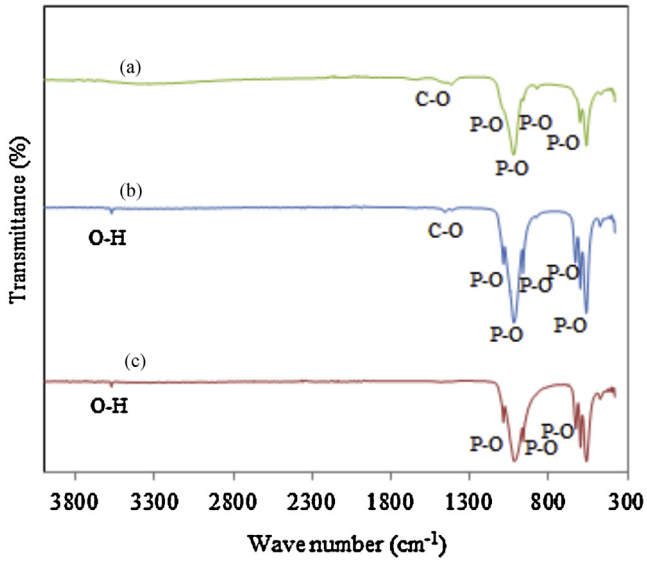

Fig. 6 – FTIR spectra for the three different HAP powders: (a) as-synthesised HAP, (b) heat treated HAP, and (c) Commercial HAP.

PO_4^{3-} and OH^{-1} groups characteristic of HAP: the bands at 962, 874 and 559 cm^{-1} correspond to the PO_4^{3-} group (Tanaka et al., 2012; Reddy et al., 2007; Wang et al., 2010). Based on several studies done on HAP as photocatalyst, the PO_3^{4-} group is believed to play important roles in the photocatalytic reactions (Nishikawa, 2004a; Pratap Reddy et al., 2007; Reddy et al., 2007). The electron state of the surface PO_3^{4-} group changes and create a vacancy on the HAP and consequently will cause the formation of $O_2^{\bullet-}$ through the electron transfer to O_2 in the atmosphere. The FTIR spectra of the as-synthesised HAP (Fig. 6a), showed a broad band around 3300 cm^{-1} which is due to absorbed water, whereas this broad band does not appear in either the heat treated or the commercial HAP. This shows that this water is not strongly bound and can be removed via drying if this is needed. The IR spectra for both the heat treated and commercial HAP (Fig. 6b) show a band around 3572 cm^{-1} assigned to the hydroxyl group (Tanaka et al., 2012; Wang et al., 2010). Based on the study done by Tanaka et al. (2012), this hydroxyl group played an important role in the photocatalytic decomposition of dimethyl sulphide, where this decomposition through UV irradiation took place on the surface P–OH groups of HAP, which may be due to the formation of surface P–OH radicals.

The intense sharp bands around 1087, 962, 600 and 474 cm^{-1} seen in both the heat treated and commercial HAP, which correspond to the PO_4^{3-} group, confirm that the HAP synthesised from the shell waste material was similar to that of the commercial powder. From the EDS spectrum for the as-synthesised and heat treated HAP, shown in Fig. 7a and b respectively, it can be seen that both materials are composed of calcium, carbon, oxygen and phosphorous. However, traces of potassium were also observed in both samples. This is perhaps due to the material being insufficiently washed with water and future work will look at optimising this washing stage. It is important to wash the precipitate with high water purity because the apatite lattice readily incorporates foreign elements into the structure (Gross and Berndt, 2002).

From the EDS analysis, the Ca/P ratio for both samples were calculated and for the as-synthesised HAP, the Ca/P ratio was 1.61 while for the heat treated sample the ratio was 1.66 which is very close to the stoichiometric HAP ratio of 1.67.

3.3. *Photocatalytic degradation of methylene blue by HAP*

The results of the degradation of methylene blue in photolysis (UV lit in the absence of catalyst), under dark (i.e. adsorption only) and with UV lit oxygen limited and oxygen rich conditions are shown in Fig. 8.

Fig. 8 shows that photolysis of methylene blue was negligible, indicating that the degradation of methylene blue in the presence of HAP is likely to be due to photocatalysis. The photolytic degradation of methylene blue in this reactor has been also shown to be negligible in previous work in the same laboratory (Ali et al., 2010).

The dark adsorption experiments shown in Fig. 8 show that adsorption to the HAP at the loading used (methylene blue at 5 $mg\,L^{-1}$ and heat treated HAP at 2.0 g/L) was negligible. This indicates that adsorption is likely to be a minor methylene blue removal mechanism in this system (assuming that adsorption properties do not change significantly in the presence of UV light).

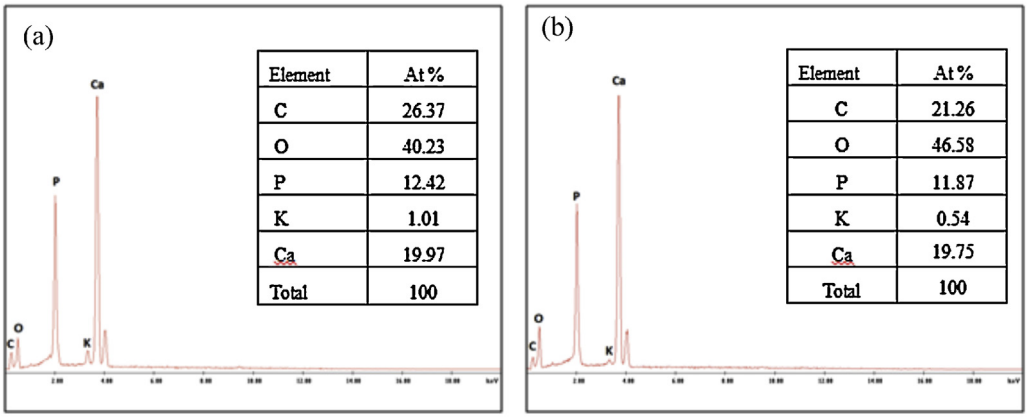

Fig. 7 – EDS analysis for: (a) as-synthesised HAP and (b) heat treated HAP.

When UV light (at 254 nm) was present, photocatalysis occurred under both oxygen rich and oxygen limited conditions. Degradation (here monitored via decolorisation at a UV–vis wavelength of 662 nm which is characteristic of the primary degradation of methylene blue) was observed for the first 90 min only with an overall degradation of only 1.8% and no further decrease with time. It can be seen that the degradation was higher when oxygen (the oxidant) is present and the reasons for this are discussed below. Under oxygen limited conditions the degradation was around 39% after 6 h and showed no further change when extending the time to 24 h. For the oxygen rich conditions, at 6 h the degradation was around 54% and increased further with time, reaching 62% after 24 h.

Overall Fig. 8 therefore shows that HAP derived from mussel shells is a photocatalyst in the presence of UV light when used in aqueous solutions. This therefore opens up the possibilities of using HAP for pollution remediation through the transformation of a significant existing waste material – waste sea shells. Furthermore, this shows that a greener photocatalyst is available, produced from readily and widely available atoms and synthesised from renewable and potentially recycled sources (if for example the phosphates are taken from wastewaters). However, the key issue is – how good a photocatalyst is it?

When compared to another HAP, the shell-derived HAP appears to be a superior photocatalyst. Fig. 9 shows a comparison of mussel shell derived heat treated HAP and the Sulzer Metco commercially sourced HAP for the photocatalytic degradation of methylene blue under oxygen rich conditions. This shows that the mussel shell derived HAP is the more effective photocatalyst over the reaction period studied. The difference in performance between the two is most likely due to the differences in material properties outlined in Sections 3.1 and 3.2. It is suspected that the difference in performance is from the CO_3^{2-} ions in the shell-derived heat treated HAP as shown

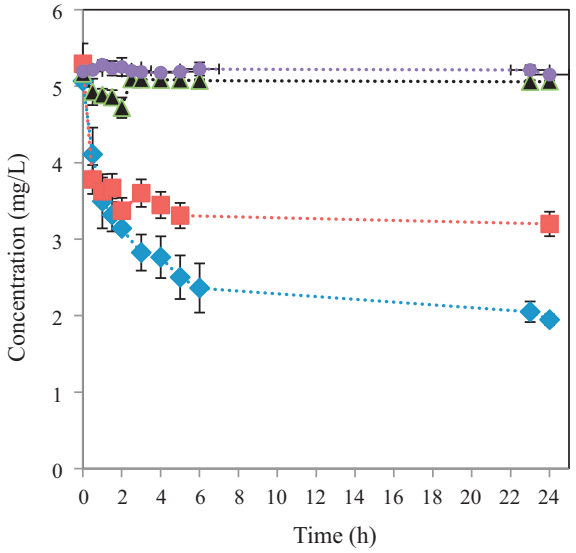

Fig. 8 – Comparison of the degradation of the azo dye compounds from methylene blue and its reaction intermediates using UV–vis spectroscopy in: photolysis control experiments under oxygen rich conditions (●), adsorption (UV dark) control experiments under oxygen rich conditions (▲), heat treated HAP photocatalysis under oxygen limited conditions (■), heat treated HAP photocatalysis under oxygen rich conditions (♦). HAP loaded at 2.0 g/L.

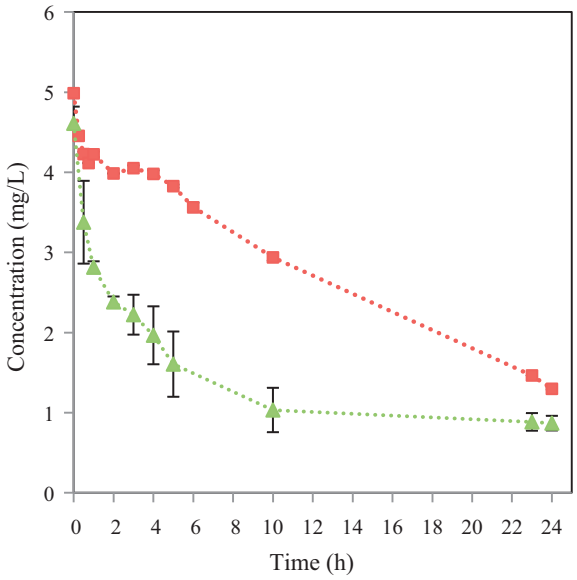

Fig. 9 – Comparison of the Sulzer Metco commercially sourced HAP (■) and mussel shell derived heat treated HAP (▲) for the photocatalytic degradation under oxygen rich conditions of methylene blue and its azo dye reaction products with concentration of the azo dyes measured using UV–vis spectroscopy. Both catalysts were loaded at 2.5 g/L.

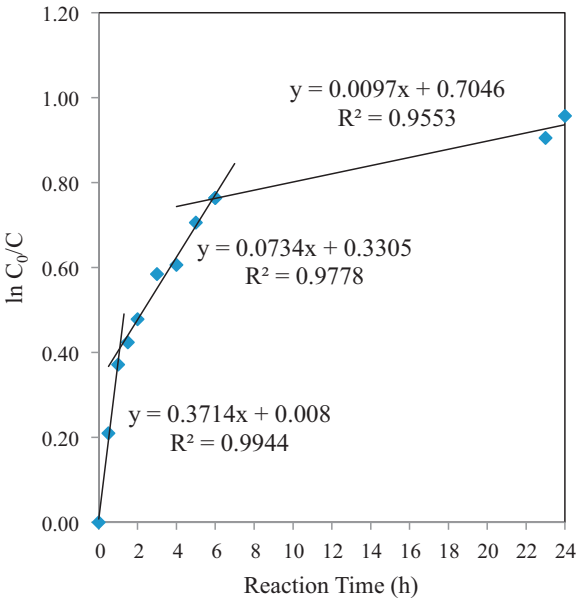

Fig. 10 – Three stage first order plot for the kinetic photodegradation of azo dye in the presence of heat treated HAP as photocatalyst under oxygen rich conditions based on the data in Fig. 8.

in Fig. 6b. The exact nature of this performance enhancement has yet to be determined.

A kinetic analysis of the data with the heat treated HAP as photocatalyst in Fig. 8 is shown in Fig. 10 and Table 2. A first order kinetic model analysis is used as these are commonly used in photocatalysis research (as the simplification of the Langmuir–Hinshelwood kinetic model when there are dilute reactant concentrations) and have in particular been used in several studies quantifying the kinetics of photocatalytic dye oxidation in aqueous systems (Houas et al., 2001; Rauf et al., 2010). Fig. 10 is the resulting first-order-reaction analysis of methylene blue degradation with heat treated HAP. Note that the semi log data does not produce a single straight line, hence does not fit a simple first order reaction model for the entire period of the reaction. A series of first order reactions (as shown in Fig. 10) is often found to be appropriate for advanced oxidation reactions, since the degradation can be broken down in to several different dominant reaction steps, such as primary degradation of the reactant, several secondary degradation steps corresponding to the oxidation to major stable/recalcitrant classes of reaction intermediate and finally mineralisation (Houas et al., 2001; Ali et al., 2011). This is an accepted kinetic modelling strategy for both non-catalytic and heterogeneously catalysed wet oxidation reactions (Li et al., 1991; Belkacemi et al., 2000), a technology which also degrades compounds via a free radical oxidation mechanism (Patterson et al., 2001b). It is not widely used for photocatalysis since the primary degradation of the reactant is often dominant and so fast that many reactions can be fitted with a single first order expression – this is however not the case for the HAP photocatalysis reactions here and so the reactions of the intermediates need to be accounted for in the kinetics. It is found that the degradation of methylene blue and its azo dye reaction intermediates is well modelled by a three step series of first order reactions. This reflects the expected reaction pathway: first from methylene blue to azo dye intermediates (which should have the fastest rate, since methylene blue has the strongest response in the UV–vis measurement used in this work), then secondary degradation of the azo dyes to smaller more highly oxidised intermediates (that do not show UV absorbance at 662 nm) and finally degradation of the recalcitrant coloured reaction intermediates. This directly relates to the currently understood pathways of methylene blue photocatalytic degradation (Ali et al., 2011). Fig. 11 shows the concentration of MB and the peak areas of the reaction intermediates/products as measured by HPLC during the course of a typical reaction and indicates that these pathways most likely apply for the photcatalysis of MB with HAP also. In particular, these results show that like many other studies of the photocatalytic degradation of MB, Azure B is the major reaction intermediate/product (Ali et al., 2011). Fig. 11 also indicates that the reaction rate for all of the component reactions slows considerably between the 5 and 10 h reaction time – this is inclusive of the degradation of MB as well as the formation and degradation of Azure A, Azure B, Azure C and Thionin. A full analysis of these reaction pathways and kinetics will be covered in a future publication.

Table 2 – Summary of three steps of first order reaction rate constant on liquid volume basis (k_{app}: min^{-1}).

Reaction step	Reaction rate constant, k_{app} (min^{-1})
1	6.2×10^{-3}
2	1.2×10^{-3}
3	1.6×10^{-4} (approximate)[a]

[a] Due to lack of data over this rate period.

The first order reaction rate constants for three first order kinetic regions are shown in Table 2. These show the trend expected from the methylene blue reaction mechanism: fast primary degradation, slower secondary degradation, with the degradation of the recalcitrant intermediates being the slowest reaction stage. However it also could indicate that the reaction is either product inhibited and/or affected by catalyst deactivation – and so this was therefore investigated further. Note that due to limited data in the final stages of the reaction, the authors are less confident on the value with the rate constant for the third and final reaction stage, compared to the first two stages of the reaction. Further work is needed to refine this value. However, the rate and rate constants are representative of the overall change in concentration seen during this time and serve to demonstrate that the rate is slower during this period.

Fig. 12 shows a comparison between heat treated HAP photodegradation of MB at two different stirring speeds: 300 and 600 rpm. These results show that there is no significant difference in degradation extent and therefore reaction rate between the two sets of data (within the error range of the data). This indicates that external mass transfer resistances are not significant at the stirring speeds used. The true photocatalytic reaction kinetics have therefore been measured and quantified in the preceding analysis.

Overall, these results are consistent with the fact that dissolved oxygen should be able to scavenge an electron at the surface of a UV-irradiated photocatalyst, which aids in the separation of photo-generated charges and decreases the recombination of generated electron–hole pairs (Nishikawa and Omamiuda, 2002). In other words, oxygen provides the oxidant source in indirect oxidation through the production of radical species (most likely hydroxyl radicals here) and so having an excess of it present should increase the oxidation rate, as observed (in Fig. 8 in particular). This is well established in semiconductor photocatalysis work, but has not

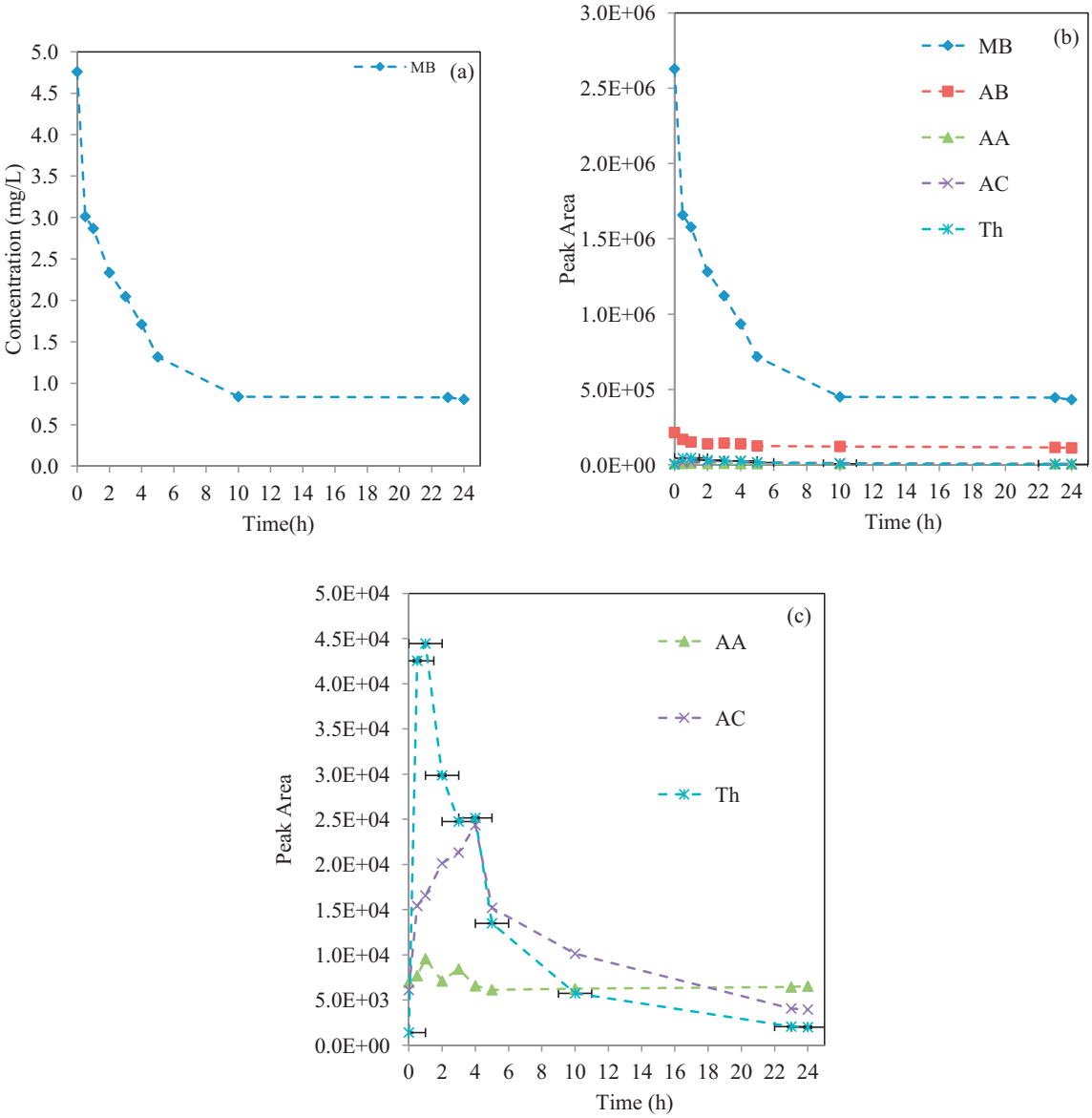

Fig. 11 – HPLC determined reaction profile of the degradation of initially 5 mg L^{-1} MB with 2.5 g/L of heat treated HAP photocatalyst under oxygen rich conditions, showing the concentration of MB and its degradation intermediates/products over the reaction period. Reaction intermediates/products are: Azure A (AA), Azure B (AB), Azure C (AC) and Thionin (Th). (a) Methylene blue concentration (b) Overall reaction profile with HPLC peak area as a proxy for concentration, (b) close-up of the intermediate/products without major reaction species MB and AB with HPLC peak area as a proxy for concentration.

yet been clearly established for liquid phase HAP photocatalysis. However, there an analogy to this in previous gaseous HAP photocatalytic work where Nishikawa and Omamiuda (2002) reported that an increase in the photocatalytic degradation of methyl mercaptane by hydroxyapatite corresponded to an increase in the amount of superoxide ($O_2^{\bullet -}$) species which were generated due to the UV irradiation – the main species that would be generated by indirect oxidation in a dry gas phase photooxidation. The formation of radicals on HAP through UV irradiation in the gas phase is also reported in other papers from the same research group (Nishikawa and Omamiuda, 2002; Nishikawa, 2003, 2004a,b, 2007). Nishikawa and Omamiuda (2002) have indicated that the oxygen vacancy is formed on HAP by UV irradiation and suggest that the activation of oxygen takes place by the formation of the labile superoxide radicals due to electron transfer to O_2 in the atmosphere (Nishikawa and Omamiuda, 2002). It is likely that in the aqueous environment of the current experiments, a similar mechanism is occurring, but with hydroxyl radical species (such as HO•) being formed instead of the superoxide radicals, as dictated by the expected aqueous equilibrium reactions of these species (Dannacher and Schlenker, 1996; Patterson et al., 2001a,b) and as found in conventional semi-conductor photocatalysis (Hoffmann et al., 1995). However, if this is the case, then this mechanism cannot be used to explain the photocatalytic reaction proceeding in the absence of sufficient oxygen, as in the oxygen limited case. Here, the only available oxygen is from the residual oxygen within the reaction solution and any that can mass transfer from the surface of the solution into the bulk solution.

Comparative FTIR spectra of the heat treated HAP powder before and after the photocatalytic reaction are shown in Fig. 13. This figure reveals that the absorbance intensity due to the PO_4^{3-} group at 1087, 960, 594 and 470 cm^{-1} are drastically decreased after photocatalytic reaction. A similar trend was observed for the band at 1019 cm^{-1} which corresponds to

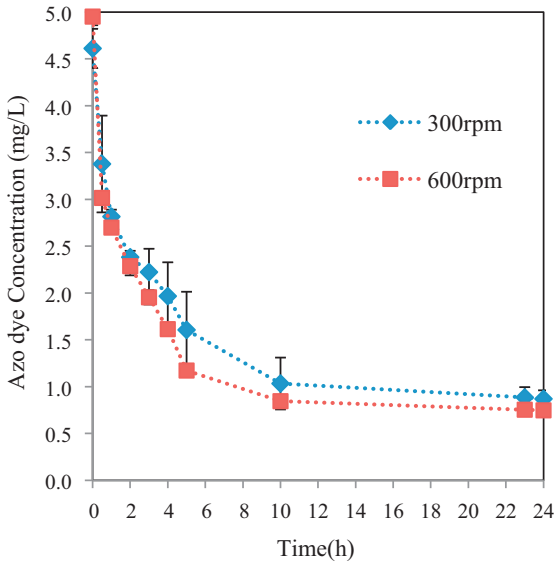

Fig. 12 – Comparison of the degradation of the azo dye compounds from methylene blue and its reaction intermediates by photocatalysis at two different stirring speeds with 2.5 g/L heat treated HAP under oxygen rich conditions with concentrations measured using UV–vis spectroscopy. This shows that external mass transfer resistances are likely to be insignificant at the stirring speeds used.

the HPO_4^{2-} in non-stoichiometric HAP. The formation of radicals on HAP by a photocatalytic reaction has been reported by several researchers. The changes of surface PO_4^{3-} group and generation of trapped electron suggest the appearance of oxygen vacancy by UV irradiation (Nishikawa and Omamiuda, 2002; Nishikawa, 2003, 2004a). This indicates that the phosphate group (the moiety containing oxygen in HAP) could be dissolved during the reaction. This is not expected at the pH that the HAP was subjected to in this reaction (the pH of the solution before the photocatalytic reaction was 6.7 and following the reaction was slightly higher at 7.8), since HAP is sparingly soluble at pHs above 4.2 (De Groot et al., 1990; Ferna'ndez et al., 1999). This may therefore indicate that there is photocatalytic dissolution of HAP. Furthermore, since there

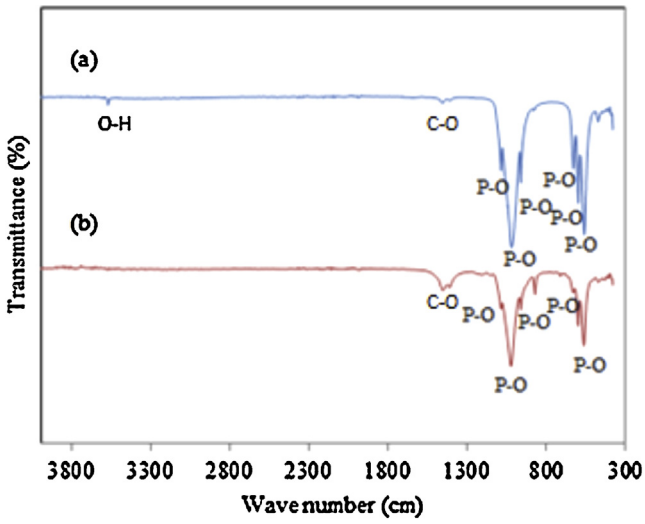

Fig. 13 – FTIR spectra for the heat treated HAP powder: (a) before photocatalytic reaction and (b) after photocatalytic reaction.

is photocatalytic activity in the absence of an oxidant, this may also indicate that the lattice oxygen is being used instead, in a Mars Van Krevelen type mechanism. A parallel to this lies in the work of Ali et al. (2010, 2011) who used nanostructured ZnO thin films in methylene blue photocatalysis. In this work, it was demonstrated that photocatalysis occurred in the absence of oxidant (as it does here) and through confirming more rapid dissolution of the ZnO under these conditions, it was hypothesised that this was likely to be through a Mars Van Krevelen type mechanism, where lattice oxygen from the ZnO films were consumed under oxygen limited conditions. The effect was more pronounced in less crystalline structures (i.e. more defects, which aid photo-dissolution). Similar results are seen in this work, so it is therefore possible that the same may also be happening with the HAP here.

Therefore, the decrease in the absorbance intensity due to PO_4^{3-} and HPO_4^{2-} in Fig. 13 may indicate that these groups are being photo-dissolved in order for the lattice oxygen to participate in the redox reactions degrading the methylene blue. This is perhaps due to the trapped electron generated by the UV irradiation forming surface P–OH radicals on HAP. This photo-degradation would also deactivate the HAP photocatalyst, which may also be a contributing factor to the drop in reaction rate in the latter stages of the reaction as outlined earlier.

This all indicates that like the ZnO photocatalysts, the HAP photocatalytic reaction mechanism in both the solid and liquid phases are not fully understood and is different to what is expected from the currently available photocatalysis literature. Further work is therefore continuing, characterising a full range of HAP structures and photocatalytic reaction mechanisms in both the solid and liquid phases, determining the optimal conditions and operating envelope for stabilising this photocatalyst deactivation pathway whilst maintaining acceptable photocatalytic activity.

4. Conclusions

It has been demonstrated that it is possible to use waste mussel shells (*Perna canaliculus*) as a calcium source to form lime (calcium oxide) and then hydroxyapatite (HAP) by first pyrolysis at 800 °C and then a wet precipitation method at room temperature and without pH control in a short 5 h reaction time. A further heat treatment at 800 °C increased the crystallinity of the HAP formed. The HAP produced was comparable to a commercial HAP, although the as-synthesised material contained residual calcite due to incomplete calcination. This calcite was removed by the subsequent heat treatment step following HAP production.

It has been shown for the first time that this mussel derived HAP can be used as a photocatalyst for the degradation of aqueous pollutants. Methylene blue was successfully degraded (primarily measured as decolourization at a UV–vis wavelength of 662 nm) by the heat treated HAP photocatalyst under both oxygen limited and oxygen rich conditions. Under oxygen limited conditions, the degradation of methylene blue was approximately 39% after 6 h and showed no further increase with longer durations. For the oxygen rich conditions, degradation during the initial 6 h was approximately 54% and increased to 62% after 24 h. The photodegradation of methylene blue in the presence of HAP as photocatalyst is well modelled by a series of three first-order-reactions with the first stage reaction rate constant is $6.2 \times 10^{-3}\,min^{-1}$,

followed by 1.2×10^{-3} min^{-1} for the second stage and finally approximately (due to limited data in this kinetic stage) 1.6×10^{-4} min^{-1} for the third stage with an average reaction rate of 2.5×10^{-8} mol L^{-1} min^{-1} over all three stages. These three reaction stages reflect the currently understood photocatalytic reaction pathway: primary degradation of methylene blue to azo dye intermediates, then secondary degradation to smaller more highly oxidised intermediates and finally degradation of recalcitrants. The final two steps of the reaction had significantly slower rates than the initial step, which tie in with this mechanism, however it also could indicate that the reaction is either product inhibited and/or affected by catalyst deactivation. FTIR analysis of the HAP before and after the photocatalysis experiments showed a decrease in the absorbance intensity of PO_4^{3-} and HPO_4^{2-}, indicating photo-dissolution of the HAP. This is perhaps due to trapped electrons generated by the UV irradiation forming surface P–OH$^{\bullet}$ radicals on HAP, which can participate as the oxygen and/or oxidant source for the reactions under oxygen limited conditions, but therefore also causing catalyst deactivation through dissolution. This indicates that the photocatalytic reaction mechanism in both the solid and liquid phases is different to what is normally expected from the currently available photocatalysis literature, providing a platform for future work exploring the materials and operating envelopes for stabilising this photocatalyst deactivation pathway whilst maintaining acceptable photocatalytic activity.

Overall this project indicates that waste mussel shells can be converted into a HAP photocatalyst with good photocatalytic activity. This potentially provides a greener route for recovering and recycling waste shells into hydroxyapatite which can be used as alternative photocatalyst in the photocatalytic degradation of wastewater components.

Acknowledgements

The authors acknowledge the PhD scholarship by Ministry of Higher Education, Malaysia and the support of Universiti Malaysia Pahang. The authors thank Raymond Hoffmann, Peter Buchanan, Catherine Hobbis, Laura Liang, Jessie Matthew, Cecilia Lourdes, Allan Clendinning, Alec Asadov, Steve Strover and Frank Wu from the Department of Chemical and Materials Engineering at the University of Auckland for their help in this work. Finally, thank you to Sanford Limited (NZ) for donating the mussel shells used in this work.

Appendix A. Supplementary data

Supplementary data associated with this article can be found, in the online version, at doi:10.1016/j.cherd.2013.04.018.

References

Abeynaike, A., Hanley, B., Wang, L., Jones, M.I., Patterson, D.A., 2008. Investigating the potential of using mussel shells for the synthesis of hydroxyapatite. In: Chemeca 2008 (36th: 2008: Newcastle, NSW), Engineers Australia [Barton, ACT], pp. 615–629.

Abeynaike, A., Wang, L., Jones, M.I., Patterson, D.A., 2011. Pyrolysed powdered mussel shells for eutrophication control: effect of particle size and powder concentration on the mechanism and extent of phosphate removal. Asia-Pac. J. Chem. Eng. 6, 231–243.

Akpan, U.G., Hameed, B.H., 2009. Parameters affecting the photocatalytic degradation of dyes using TiO_2-based photocatalysts: a review. J. Hazard. Mater. 170, 520–529.

Ali, A.M., Emanuelsson, E.A.C., Patterson, D.A., 2011. Conventional versus lattice photocatalysed reactions: implications of the lattice oxygen participation in the liquid phase photocatalytic oxidation with nanostructured ZnO thin films on reaction products and mechanism at both 254 nm. Appl. Catal. B: Environ. 106, 323–336.

Ali, A.M., Emanuelsson, E.A.C., Patterson, D.A., 2010. Photocatalysis with nanostructured zinc oxide thin films: the relationship between morphology and photocatalytic activity under oxygen limited and oxygen rich conditions and evidence for a Mars Van Krevelen mechanism. Appl. Catal. B: Environ., 168–181.

Al-Qasas, N.S., Rohani, S., 2005. Synthesis of pure hydroxyapatite and the effect of synthesis conditions on its yield, crystallinity, morphology and mean particle size. Sep. Sci. Technol. 40, 3187–3224.

Belkacemi, B., Larachi, F., Sayari, A., 2000. Lumped kinetics for solid-catalyzed wet oxidation: a versatile model. J. Catal. 193, 224–237.

Boiarkina, I., Pedron, S., Patterson, D.A., 2011. An experimental and modelling investigation of the effect of the flow regime on the photocatalytic degradation of methylene blue on a thin film coated ultraviolet irradiated spinning disc reactor. Appl. Catal. B: Environ. 110, 14–24.

Boucetta, C., Kacimi, M., Ensuque, A., Piquemal, J.-Y., Bozon-Verduraz, F., Ziyad, M., 2009. Oxidative dehydrogenation of propane over chromium-loaded calcium-hydroxyapatite. Appl. Catal. A: Gen. 356, 201–210.

Castello, G.K., 2009. Handbook of Photocatalysts: Preparation Structure and Applications. Nova Science Pub Incorporated.

Chong, M.N., Jin, B., Chow, C.W.K., Saint, C., 2010. Recent developments in photocatalytic water treatment technology: a review. Water Res. 44, 2997–3027.

Cullity, B.D., 1956. Elements of X-Ray Diffraction. Addison-Wesley Publishing Company, Inc.

Currie, J.A., Harrison, N.R., Wang, L., Jones, M.I., Brooks, M.S., 2007. A preliminary study of processing seafood shells for eutrophication control. Asia-Pac. J. Chem. Eng. 2, 460–467.

Dannacher, J., Schlenker, W., 1996. The mechanism of hydrogen peroxide bleaching. Text. Chem. Color. 28, 24–28.

Davis, B.L., Adams, L.H., 1965. Kinetics of the calcite ⇌ aragonite transformation. J. Geophys. Res. 70, 433–441.

De Groot, K., Klein, C., Wolke, J., de Blieck-Hogervorst, J., 1990. Chemistry of calcium phosphate bioceramics. In: Yamamuro, T., Hench, L., Wilson, J. (Eds.), Handbook of bioactive ceramics, Vol. II. CRC Press, Boca Raton, FL, pp. 3–16.

De Lasa, H.I., Serrano, B., Salaices, M., 2005. Photocatalytic Reaction Engineering. Springer.

Domínguez, M.I., Romero-Sarria, F., Centeno, M.A., Odriozola, J.A., 2009. Gold/hydroxyapatite catalysts: synthesis, characterization and catalytic activity to CO oxidation. Appl. Catal. B: Environ. 87, 245–251.

Ferna'ndez, E., Gil, F.J., Ginebra, M.P., Driessens, F.C.M., Planell, J.A., Best, S.M., 1999. Calcium phosphate bone cements for clinical applications. Part I: solution chemistry. J. Mater. Sci. Mater. Med. 10, 169–176.

Galvan-Ruiz, M., Hernandez, J., Banos, L., Noriega-Montes, J., Rodriguez-Garcia, M.E., 2009. Characterization of calcium carbonate, calcium oxide, and calcium hydroxide as starting point to the improvement of lime for their use in construction. J. Mater. Civ. Eng. 21, 694–698.

Gaya, U.I., Abdullah, A.H., 2008. Heterogeneous photocatalytic degradation of organic contaminants over titanium dioxide: a review of fundamentals progress and problems. J. Photochem. Photobiol. C: Photochem. Rev. 9, 1–12.

Gross, K.A., Berndt, C.C., 2002. Biomedical Application of Apatites. Rev. Mineral. Geochem. 48, 631–672.

Hoffmann, M.R., Martin, S.T., Choi, W., Bahnemann, D.W., 1995. Environmental applications of semiconductor photocatalysis. Chem. Rev. 95, 69–96.

Houas, A., Lachheb, H., Ksibi, M., Elaloui, E., Guillard, C., Herrmann, J.-M., 2001. Photocatalytic degradation pathway of methylene blue in water. Appl. Catal. B: Environ. 31, 145–157.

Hu, A., Li, M., Chang, C., Mao, D., 2007. Preparation and characterization of a titanium-substituted hydroxyapatite photocatalyst. J. Mol. Catal. A: Chem. 267, 79–85.

Ji, S., Murakami, S., Kamitakahara, M., Ioku, K., 2009. Fabrication of titania/hydroxyapatite composite granules for photo-catalyst. Mater. Res. Bull. 44, 768–774.

Jones, M.I., Wang, L.Y., Abeynaike, A., Patterson, D.A., 2011. Utilisation of waste material for environmental applications: calcination of mussel shells for waste water treatment. Adv. Appl. Ceram. 110, 280–286.

Jun, J.H., Lee, T.-J., Lim, T.H., Nam, S.-W., Hong, S.-A., Yoon, K.J., 2004. Nickel-calcium phosphate/hydroxyapatite catalysts for partial oxidation of methane to syngas: characterization and activation. J. Catal. 221, 178–190.

Khalid, M., Mujahid, M., Amin, S., Rawat, R.S., Nusair, A., Deen, G.R., 2013. Effect of surfactant and heat treatment on morphology, surface area and crystallinity in hydroxyapatite nanocrystals. Ceram. Int. 39, 39–50.

Khachani, M., Kacimi, M., Ensuque, A., Piquemal, J.-Y., Connan, C., Bozon-Verduraz, F., Ziyad, M., 2010. Iron-calcium-hydroxyapatite catalysts: iron speciation and comparative performances in butan-2-ol conversion and propane oxidative dehydrogenation. Appl. Catal. A: Gen. 388, 113–123.

Khataee, A.R., Kasiri, M.B., 2010. Photocatalytic degradation of organic dyes in the presence of nanostructured titanium dioxide: influence of the chemical structure of dyes. J. Mol. Catal. A: Chem. 328, 8–26.

Koutsopoulos, S., 2002. Synthesis and characterization of hydroxyapatite crystals: a review study on the analytical methods. J. Biomed. Mater. Res. 62, 600–612.

Kuriyavar, S.I., Vetrivel, R., Hegde, S.G., Ramaswamy, A.V., Chakrabarty, D., Mahapatra, S., 2000. Insights into the formation of hydroxyl ions in calcium carbonate: temperature dependent FTIR and molecular modelling studies. J. Mater. Chem. 10, 1835–1840.

Li, L., Chen, P., Gloyna, E.F., 1991. Generalized kinetic model for wet oxidation of organic compounds. AIChE J. 37, 1687–1697.

Liu, Y., Liu, C.Y., Wei, J.H., Xiong, R., Pan, C.X., Shi, J., 2010. Enhanced adsorption and visible-light-induced photocatalytic activity of hydroxyapatite modified Ag-TiO_2 powders. Appl. Surf. Sci. 256, 6390–6394.

Mills, A., Le Hunte, S., 1997. An overview of semiconductor photocatalysis. J. Photochem. Photobiol. A: Chem. 108, 1–35.

Mills, A., 2012. An overview of the methylene blue ISO test for assessing the activities of photocatalytic films. Appl. Catal. B: Environ. 128, 144–149.

Mostafa, N.Y., 2005. Characterization, thermal stability and sintering of hydroxyapatite powders prepared by different routes. Mater. Chem. Phys. 94, 333–341.

Nan, Z., Shi, Z., Yan, B., Guo, R., Hou, W., 2008. A novel morphology of aragonite and an abnormal polymorph transformation from calcite to aragonite with PAM and CTAB as additives. J. Colloid Interface Sci. 317, 77–82.

Nishikawa, H., 2003. Surface changes and radical formation on hydroxyapatite by UV irradiation for inducing photocatalytic activation. J. Mol. Catal. A: Chem. 206, 331–338.

Nishikawa, H., 2004a. A high active type of hydroxyapatite for photocatalytic decomposition of dimethyl sulfide under UV irradiation. J. Mol. Catal. A: Chem. 207, 149–153.

Nishikawa, H., 2004b. Radical generation on hydroxyapatite by UV irradiation. Mater. Lett. 58, 14–16.

Nishikawa, H., 2007. Photo-induced catalytic activity of hydroxyapatite based on photo-excitation. Phosphorus Res. Bull. 21, 97–102.

Nishikawa, H., Omamiuda, K., 2002. Photocatalytic activity of hydroxyapatite for methyl mercaptane. J. Mol. Catal. A: Chem. 179, 193–200.

Parker, J.E., Thompson, S.P., Lennie, A.R., Potter, J., Tang, C.C., 2010. A study of the aragonite-calcite transformation using Raman spectroscopy, synchrotron powder diffraction and scanning electron microscopy. CrystEngComm 12, 1590–1599.

Patterson, D.A., Metcalfe, I.S., Xiong, F., Livingston, A.G., 2001a. Wet air oxidation of linear alkylbenzene sulfonate 1. Effect of temperature and pressure. Ind. Eng. Chem. Res. 40, 5507–5516.

Patterson, D.A., Metcalfe, I.S., Xiong, F., Livingston, A.G., 2001b. Wet air oxidation of linear alkylbenzene sulfonate 2. Effect of pH. Ind. Eng. Chem. Res. 40, 5517–5525.

Perić, J., Vučak, M., Krstulović, R., Brečević, L., Kralj, D., 1996. Phase transformation of calcium carbonate polymorphs. Thermochim. Acta 277, 175–186.

Pratap Reddy, M., Venugopal, A., Subrahmanyam, M., 2007. Hydroxyapatite-supported Ag-TiO_2 as *Escherichia coli* disinfection photocatalyst. Water Res. 41, 379–386.

Rakovan, J., 2002. Growth and surface properties of apatite. Rev. Mineral. Geochem. 48, 51–86.

Rauf, M.A., Meetani, M.A., Khaleel, A., Ahmed, A., 2010. Photocatalytic degradation of methylene blue using a mixed catalyst and product analysis by LC/MS. Chem. Eng. J. 157, 373–378.

Reddy, M.P., Venugopal, A., Subrahmanyam, M., 2007. Hydroxyapatite photocatalytic degradation of calmagite (an azo dye) in aqueous suspension. Appl. Catal. B: Environ. 69, 164–170.

Resende, N.S., Nele, M., Salim, V.M.M., 2006. Effects of anion substitution on the acid properties of hydroxyapatite. Thermochim. Acta 451, 16–21.

Rodriguez-Lorenzo, L., Vallet-Regi, M., 2000. Controlled crystallization of calcium phosphate apatites. Chem. Mater. 12, 2460–2465.

Sheng, G., Qiao, L., Mou, Y., 2011. Preparation of TiO_2/hydroxyapatite composite and its photocatalytic degradation of methyl orange. J. Environ. Eng. 137, 611–616.

Sivakumar, M., Manjubala, I., 2001. Preparation of hydroxyapatite/fluoroapatite-zirconia composites using Indian corals for biomedical applications. Mater. Lett. 50, 199–205.

Solhy, A., Tahir, R., Sebti, S., Skouta, R., Bousmina, M., Zahouily, M., Larzek, M., 2010. Efficient synthesis of chalcone derivatives catalyzed by re-usable hydroxyapatite. Appl. Catal. A: Gen. 374, 189–193.

Soon, A.N., Hameed, B.H., 2011. Heterogeneous catalytic treatment of synthetic dyes in aqueous media using Fenton and photo-assisted Fenton process. Desalination 269, 1–16.

Tanaka, H., Tsuda, E., Nishikawa, H., Fuji, M., 2012. FTIR studies of adsorption and photocatalytic decomposition under UV irradiation of dimethyl sulfide on calcium hydroxyapatite. Adv. Powder Technol. 23, 115–119.

Tsuchida, T., Kubo, J., Yoshioka, T., Sakuma, S., Takeguchi, T., Ueda, W., 2008. Reaction of ethanol over hydroxyapatite affected by Ca/P ratio of catalyst. J. Catal., 183–189.

Wang, P., Li, C., Gong, H., Jiang, X., Wang, H., Li, K., 2010. Effects of synthesis conditions on the morphology of hydroxyapatite nanoparticles produced by wet chemical process. Powder Technol. 203, 315–321.

Zahouily, M., Abrouki, Y., Bahlaouan, B., Rayadh, A., Sebti, S., 2003. Hydroxyapatite: new efficient catalyst for the Michael addition. Catal. Commun. 4, 521–524.

Zhang, Y., Li, Z., Sun, W., Xia, C., 2008. A magnetically recyclable heterogeneous catalyst: cobalt nano-oxide supported on hydroxyapatite-encapsulated [gamma]-Fe_2O_3 nanocrystallites for highly efficient olefin oxidation with H_2O_2. Catal. Commun. 10, 237–242.